Nano Research

Open Access

Research Article

Competitive coordination enhancing the thermal stability of PDOL electrolytes for safe solid-state lithium metal batteries

Ying-Ying Pei[1,2,§], Jiang-Kui Hu[1,2,§], Hong Yuan[1,2] ✉, Shi-Jie Yang[1,2], Xi-Long Wang[1,2], Zheng Liao[1,2], Jia Liu[3], Bo-Quan Li[1,2] ✉, and Jia-Qi Huang[1,2] ✉

[1] *School of Materials Science and Engineering, Beijing Institute of Technology, Beijing 100081, China*
[2] *Advanced Research Institute of Multidisciplinary Science, Beijing Institute of Technology, Beijing 100081, China*
[3] *College of Materials Science and Technology, Beijing Forestry University, Beijing 100083, China*
[§] *Ying-Ying Pei and Jiang-Kui Hu contributed equally to this work.*

Cite this article: *Nano Research*, **2025**, *18*, 94907220. https://doi.org/10.26599/NR.2025.94907220

ABSTRACT: Poly(1,3-dioxolane) (PDOL)-based solid electrolytes hold great potential for solid-state lithium (Li) metal batteries due to their superior ionic conductivity at room temperature. However, traditional PDOL electrolytes suffer from inferior thermal stability, which has hampered their practical application. In this work, a competitive coordination mechanism is proposed to strengthen vulnerable ether oxygen bonds in PDOL chains, thereby improving the thermal stability of PDOL electrolytes. The strong coordination of Lewis base ligands on $Li_{6.75}La_3Zr_{1.75}Ta_{0.25}O_{12}$ (LLZTO) surface with Li ions weakens the ionic-dipolar interactions between PDOL chains and Li ions, conversely reinforcing the bond energy of ether oxygen bonds. Incorporating LLZTO into PDOL electrolytes effectively enhances the thermal decomposition temperature from 110 to 302 °C. Li||$LiFePO_4$ full cell with a 12 μm ultrathin PDOL hybrid electrolyte delivers enhanced discharge capacity and extended cycling life for 100 cycles at an elevated temperature of 60 °C. This work provides critical insights into the development of thermally stable PDOL electrolytes for safe solid-state Li metal batteries.

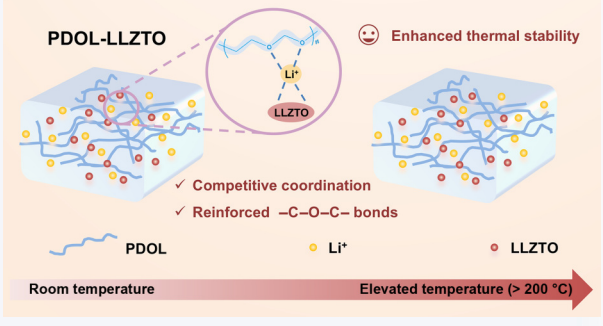

KEYWORDS: competitive coordination, solid-state battery, lithium metal, safety, electrolyte design

1 Introduction

Over the past few decades, lithium (Li)-ion batteries have dominated the energy storage market due to their low cost and long cycle life [1–3]. However, conventional Li-ion batteries, based on intercalation chemistry are approaching their theoretical energy density limits, failing to meet the escalating demand for high energy density [4–6]. Furthermore, safety concerns arising from flammable organic liquid electrolytes pose significant challenges [7–10]. Solid-state batteries, that replace organic liquid electrolytes with nonflammable solid-state electrolytes (SEs), offer a promising solution to balance safety concerns and energy density [11–14].

Polymer electrolytes, particularly *in-situ* polymerized poly(1,3-dioxolane) (PDOL) electrolytes, have gained significant attention among various SEs due to their lightweight, flexible nature, and conformal interface contact [15–17]. Besides, PDOL electrolytes exhibit remarkable room-temperature ionic conductivity of ~ 10^{-3} S·cm^{-1}, comparable to conventional liquid electrolytes [18–23]. Despite these advantages, the practical application of PDOL electrolytes has been hampered by issues such as poor thermal stability and unacceptable interface stability [24]. It is well known that pure PDOL polymer demonstrates high thermal stability, exceeding 300 °C [24]. Unfortunately, the coordination of PDOL with Li ions (Li^+) induces the transfer of the electron cloud density from the oxygen atom to Li^+, resulting in a decrease in the bond energy of the ether oxygen (–C–O–C–) bond and consequently, reduced thermal stability of PDOL [25]. The decomposition temperature of PDOL electrolytes is largely reduced to less than 120 °C [26], seriously affecting the safety of batteries. Therefore, there is an urgent need to enhance the thermal stability of PDOL electrolytes for safe Li metal batteries [20].

Several strategies have been proposed to enhance the thermal stability of PDOL electrolytes, including crosslinking

Received: November 22, 2024; **Revised:** December 23, 2024
Accepted: December 25, 2024

✉Address correspondence to Hong Yuan, yuanhong@bit.edu.cn; Bo-Quan Li, libq@bit.edu.cn; Jia-Qi Huang, jqhuang@bit.edu.cn

copolymerization and blending with inorganic fillers. For instance, a thermally stable PDOL-based electrolyte was developed through the copolymerization of DOL with 1,3-bis(3-glycidoxypropyl) tetramethyl disiloxane (PSiDOL), resulting in crosslinking frameworks that significantly increased the initial thermal decomposition temperature of PSiDOL electrolyte from 110 to 202 °C [27]. However, the design of crosslinking structures also hinders the movement of polymer segments, leading to a decrease in Li-ion conduction. The room-temperature ionic conductivity of PSiDOL electrolyte was only ~ 10^{-5} S·cm^{-1}. Another approach involves incorporating inorganic fillers into the PDOL matrix to improve thermal stability while maintaining room-temperature Li^+ conductivity. Yang et al. employed yttria-stabilized zirconia (YSZ) as functional fillers in PDOL electrolytes [25]. This approach enhanced the thermal decomposition temperature of the PDOL-YSZ electrolyte from 75 to 100 °C while retaining room-temperature ionic conductivity of 2.75 × 10^{-4} S·cm^{-1}. However, achieving intrinsic safety of PDOL electrolytes in battery energy storage systems remains a challenge. Moreover, the mechanism for enhancing the thermal stability of PDOL electrolytes is not yet clear, making it difficult to guide the rational design of PDOL electrolytes with high thermal stability.

Herein, we proposed a competitive coordination mechanism to enhance the thermal stability of PDOL electrolytes through strong Lewis acid–base interactions between Lewis base ligands and solvated Li^+. Surface Lewis base sites on $Li_{6.75}La_3Zr_{1.75}Ta_{0.25}O_{12}$ (LLZTO) competitively interact with Li^+ in the electrolyte, weakening the ionic-dipolar interactions between Li^+ and PDOL chains (Fig. 1). This, in turn, strengthens the bond energy of –C–O–C– bonds, thereby improving the thermal stability of PDOL electrolyte. The thermal decomposition temperature of PDOL hybrid electrolyte increases from 110 to 302 °C. As a result, an ultrathin PDOL hybrid electrolyte with a thickness of 12 μm and enhanced thermal stability was developed through *in-situ* polymerization of PDOL electrolyte within an ultrathin LLZTO-coated ceramic separator. The incorporation of LLZTO fillers effectively enhances the room-temperature ionic conductivity and strengthens the mechanical performance of the hybrid electrolyte. Li||$LiFePO_4$ (LFP) full cell exhibits stable cycling for 100 cycles at an elevated temperature of 60 °C. This competitive coordination mechanism opens up wide application prospects for the rational design of thermally stable PDOL electrolytes in safe solid-state Li metal batteries.

2 Results and discussion

2.1 Thermal stability and regulation mechanism of PDOL electrolyte

The thermal stability of electrolytes is a critical factor in determining the safety of batteries at high operating temperatures. In PDOL electrolyte, the coordination of PDOL chains with Li^+ induces the transfer of electron cloud density from the oxygen atom to Li^+, thereby weakening the –C–O–C– bonds and decreasing the thermal stability of PDOL electrolyte. Consequently, the PDOL electrolyte begins to decompose at approximately 98 °C, with only 50 wt.% of PDOL remaining at 133 °C (Fig. 2(a)). In contrast, the initial weight loss temperature of PDOL hybrid electrolyte containing 10 wt.% nano LLZTO with an average size of 230 nm (Fig. S1 in the Electronic Supplementary Material (ESM)) is delayed to 264 °C, and the temperature of half-decomposition remains is postponed to 305 °C. Differential scanning calorimetry (DSC) tests were conducted to further demonstrate the thermal stability of PDOL-based electrolyte. Similarly, pristine PDOL electrolyte exhibits a pronounced endothermic peak at 109 °C, attributed to the depolymerization of PDOL, while the endothermic peak of PDOL-LLZTO hybrid electrolyte rises to 302 °C (Fig. 2(b)). It is noteworthy that the mild endothermic peak below 100 °C is related to the volatilization of residual DOL solvent. Consequently, these results confirm that LLZTO significantly improves the thermal stability of the PDOL hybrid electrolyte.

To analyze the thermal decomposition behavior,

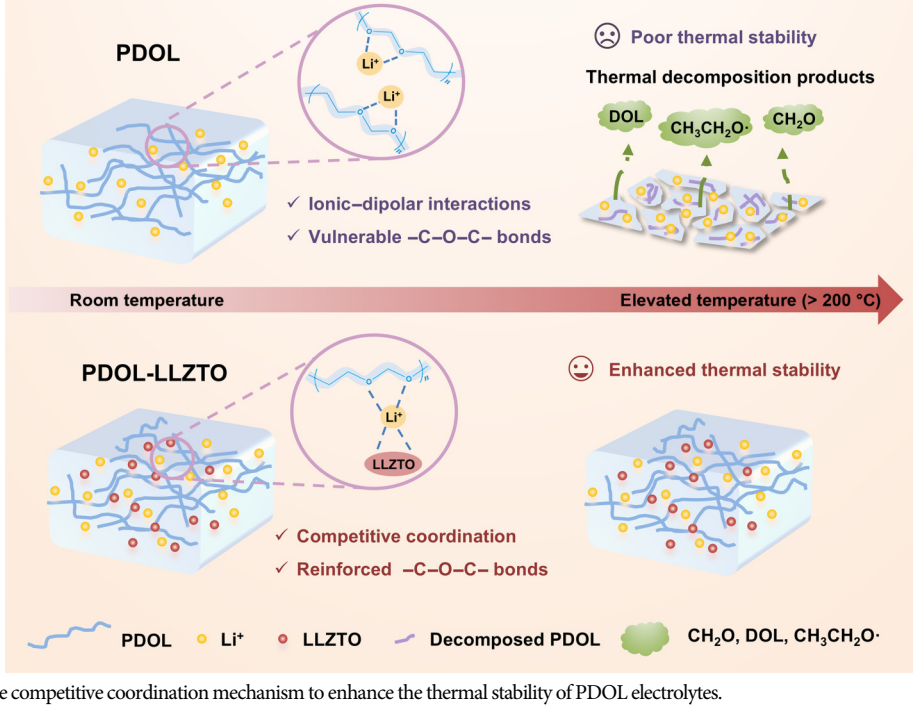

Figure 1 Illustration of the competitive coordination mechanism to enhance the thermal stability of PDOL electrolytes.

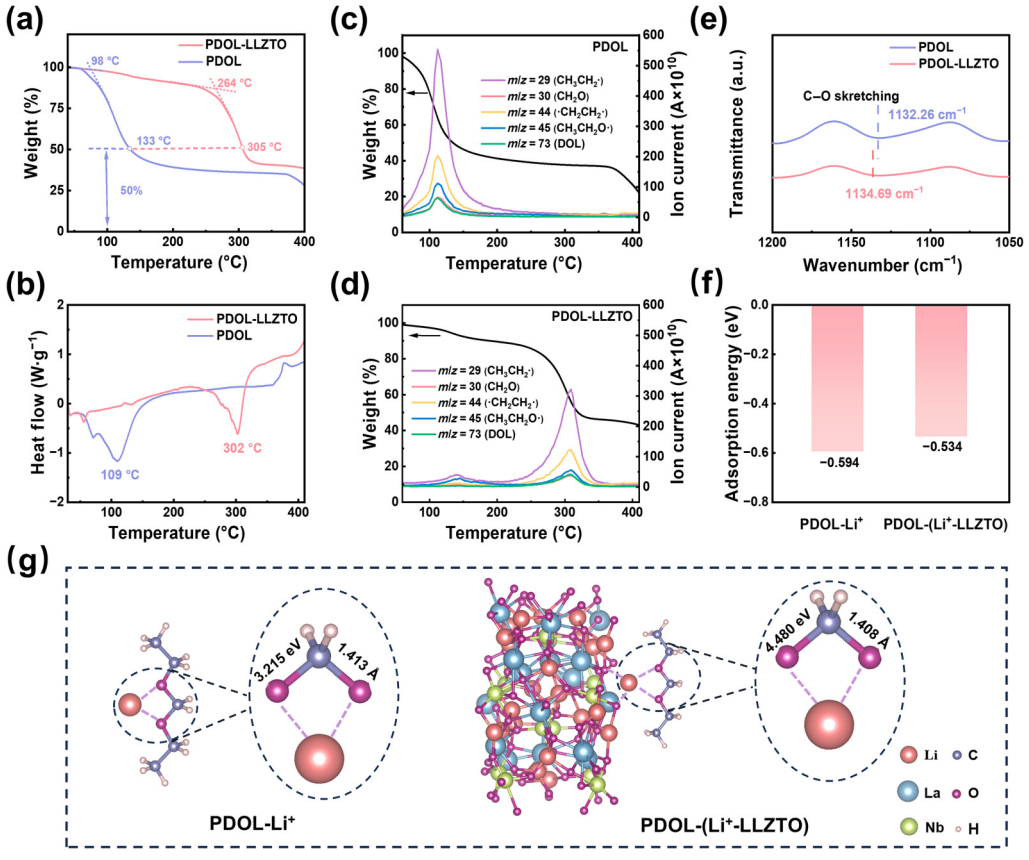

Figure 2 (a) TGA and (b) DSC curves of PDOL and PDOL-LLZTO electrolyte. TGA-MS curves of (c) PDOL and (d) PDOL-LLZTO electrolyte. (e) FT-IR spectra of the PDOL and PDOL-LLZTO electrolyte. (f) DFT calculations of adsorption energy of PDOL toward Li^+ in the PDOL-LLZTO hybrid electrolyte and (g) the corresponding bond energies and bond lengths of –C–O–C– bonds.

thermogravimetric analysis-mass spectrometry (TGA-MS) was employed to monitor the gaseous products from the decomposition of PDOL electrolyte [28, 29]. As shown in Fig. 2(c), CH_3CH_2· (m/z = 29) segments exhibit the highest ion current, indicating that the terminal ether oxygen (–O–CH_2CH_3) bonds in PDOL chains are most susceptible to cleavage. As –C–O–C– bonds are vulnerable to attack, the decomposition of PDOL also generates ·CH_2CH_2O· (m/z = 44) and CH_3CH_2O· (m/z = 45) segments. Additionally, formaldehyde (HCHO, m/z = 30) and DOL (m/z = 73) are caused by the re-coupling of the broken –O–C– bonds. Although the decomposition of PDOL-LLZTO hybrid electrolyte yields similar products, the introduction of LLZTO significantly enhances the decomposition temperature (Fig. 2(d)). This result indicates the presence of LLZTO plays a crucial role in enhancing the thermal stability of PDOL-LLZTO hybrid electrolyte.

To elucidate the mechanism by which LLZTO enhances the thermal properties of PDOL hybrid electrolyte, Fourier-transform infrared spectroscopy (FT-IR) analyses were conducted (Fig. 2(e)). The peak at 1132.26 cm^{-1} is related to the stretching vibration of –C–O–C– bonds in PDOL. Upon incorporating LLZTO into PDOL, this peak shifts to 1134.69 cm^{-1}, indicating that LLZTO strengthens the –C–O–C– bonds [25, 30]. It is well known that the surface of LLZTO possesses abundant Lewis base sites, which can coordinate with Li^+ (Lewis acid sites) in the electrolyte through Lewis acid-base interactions [31]. Thus, this reversibly weakens the coordination between –C–O–C– bonds and Li^+. In other words, the competitive coordination of LLZTO with Li^+ reinforces the bond energy of –C–O–C– bonds.

Density functional theory (DFT) calculations were further performed to investigate the interactions of Li^+ and PDOL, as well as between Li^+ and LLZTO. The adsorption energy of LLZTO with Li^+ is found to be −5.021 eV, significantly higher than that of PDOL with Li^+ at −0.594 eV (Fig. 2(f) and Fig. S2 in the ESM). This result indicates that LLZTO has a reinforced ability to competitively interact with solvated Li^+. Consequently, the adsorption energy of PDOL with Li^+ in PDOL-(Li^+-LLZTO) composite structure decreases to −0.534 eV upon involvement of LLZTO in the competitive coordination with PDOL-Li^+. The attenuated adsorption energy of PDOL with Li^+ conversely results in enhanced electron cloud density of the oxygen atom, thereby strengthening the bond energy of the –C–O–C– bond in PDOL. Consequently, the bond energy increases from 3.215 to 4.480 eV (Fig. 2(g)). Moreover, the bond length of the –C–O–C– bond decreases from 1.413 to 1.408 Å. The elevated bond energy and reduced bond length further demonstrate the enhanced thermal stability of PDOL due to the competitive interactions of LLZTO with solvated Li^+.

2.2 Preparation and properties of thermally stable PDOL hybrid electrolyte

Garnet-type LLZTO powders are widely employed as active fillers in polymer electrolytes to improve their electrochemical performance owing to their excellent thermal stability, high ionic conductivity, and good chemical stability [32]. However, the energy density, a crucial parameter of battery practical applications, is heavily dependent on the thickness of solid-state electrolyte membranes. Therefore, an ultrathin LLZTO-coated PE ceramic

separator was first prepared through ultrasonic spraying of nano LLZTO powders (Fig. S1 in the ESM) onto both sides of the ultrathin PE separator [33, 34]. In comparison to traditional tape casting, ultrasonic spray-coating can effectively suppress the aggregation of LLZTO particles, enabling the formation of a uniform LLZTO layer with controllable thickness. Subsequently, PDOL hybrid electrolyte was obtained by *in-situ* polymerization of PDOL precursor within the LLZTO-coated ceramic separator, as illustrated in Fig. 3(a). Ultrasonic spraying-coating technology, known for its uniform spray distribution and precise thickness control, is widely applied in film preparation [35]. After ultrasonic spraying, the ceramic separator is uniformly coated with nano-sized LLZTO particles (Figs. 3(b) and 3(d)). The thickness of the LLZTO layer on each side of the bare PE membrane is only 3 μm, resulting in an ultrathin LLZTO ceramic separator membrane with a total thickness of just 12 μm (Figs. 3(c) and 3(e)).

Notably, the ultrathin LLZTO coating layer acts as a rigid scaffold, not only enhancing the mechanical strength of electrolyte membranes but also preventing the thermal shrinkage of the PE separator under thermal abuse conditions, thereby averting the occurrence of internal short circuits. Nanoindentation tests demonstrate that the load-bearing capacity of the LLZTO ceramic separator stabilizes at 14.2 GPa, which is 45% higher than that of the original PE separator (Fig. 3(f)). High mechanical performance also suggests an enhanced ability to inhibit the penetration of Li dendrites during cell operation. Furthermore, the LLZTO coating layer enhances the thermal stability of the PE separator. It can be observed that the ceramic separator maintains its initial shape without obvious thermal shrinkage even at an elevated temperature of 150 °C, whereas the original PE separator undergoes severe shrinkage at 120 °C (Fig. 3(g)). This observation indicates that the LLZTO ceramic separator effectively mitigates safety hazards associated with internal short circuits under thermal abuse conditions [36].

Thermally stable and ultrathin PDOL hybrid electrolyte was synthesized through *in-situ* polymerization of PDOL precursor within LLZTO ceramic separators. Figure 4(a) illustrates the polymerization mechanism wherein the aluminum cation of aluminum trifluoromethanesulfonate ($Al(OTf)_3$) initiates the ring-opening polymerization of DOL monomers, ultimately converting it into transparent solid-state PDOL electrolyte [37]. ^{1}H nuclear magnetic resonance (NMR) spectroscopy reveals new peaks at 3.59 ppm and 4.63 ppm for PDOL and PDOL-LLZTO electrolytes, corresponding to the αH and βH atoms in PDOL, respectively (Fig. 4(b)) [24]. Similarly, ^{13}C NMR spectroscopy detects new peaks at 66.87 and 95.19 ppm, attributed to $-O-CH_2-CH_2-O-$ and $-O-CH_2-O$ groups in PDOL chains, respectively (Fig. S3 in the ESM). These results confirm the successful ring-opening polymerization of the DOL monomer. Additionally, no other characteristic peaks are observed in X-ray diffraction (XRD) spectroscopy apart from the peaks corresponding to LLZTO and PDOL (Fig. S4 in the ESM), verifying the good compatibility between LLZTO and PDOL. Moreover, the LLZTO ceramic separator exhibits a reduced contact angle and rapid wetting towards DOL precursors compared to the original PE separator, indicating excellent affinity of LLZTO with DOL (or PDOL) molecular (Fig. 4(c) and Fig. S5 in the ESM). Consequently, the porous ceramic skeletons are uniformly infiltrated by PDOL electrolyte, forming a continuous Li^+ conducting pathway (Fig. 4(d) and Fig. S6 in the ESM).

Ion conduction and Li^+ transference number (t_{Li+}) are crucial for battery performance. The Li-ion conductivity of ultrathin PDOL-LLZTO hybrid electrolyte reaches 2.12×10^{-4} S·cm^{-1} at room temperature, higher than that of pristine PDOL electrolyte (1.06 ×

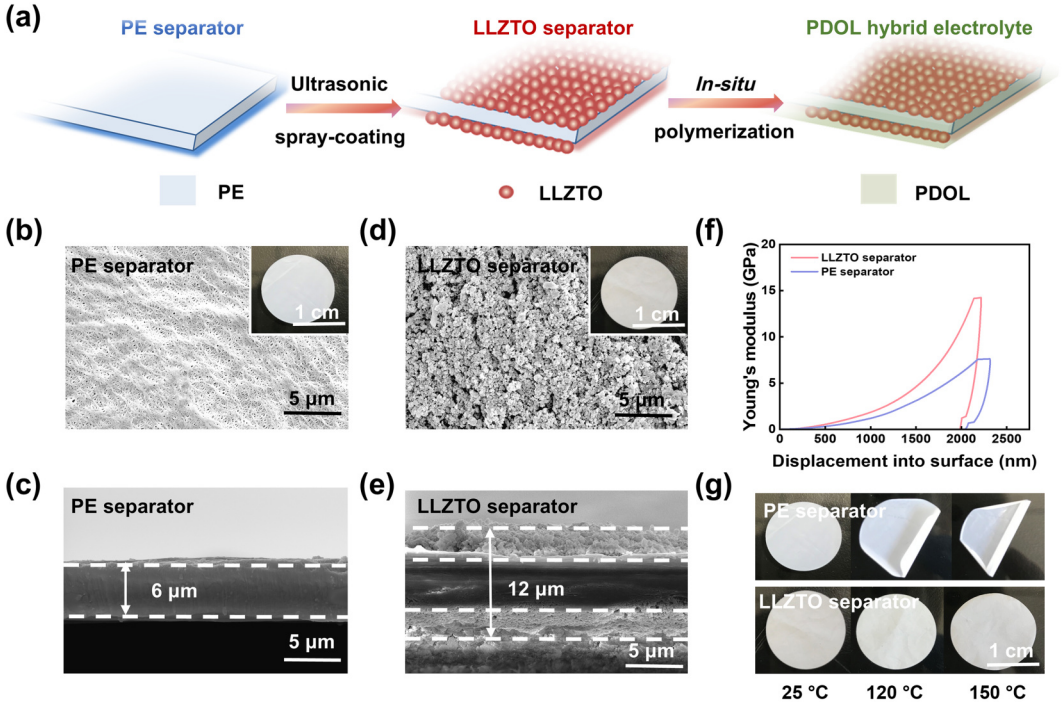

Figure 3 (a) Diagram of the preparation process of the ultrathin PDOL hybrid electrolyte. (b) and (d) Surface and optical images (inset) for the PE separator before and after ultrasonic spray-coating LLZTO nanoparticles. (c) and (e) Cross-sectional images for the PE separator before and after ultrasonic spray-coating LLZTO nanoparticles. (f) Nanoindentation profiles of original PE separator and LLZTO-coated ceramic separator. (g) Thermal shrinkage behaviors of original PE separator and LLZTO-coated ceramic separator at 25, 120, and 150 °C.

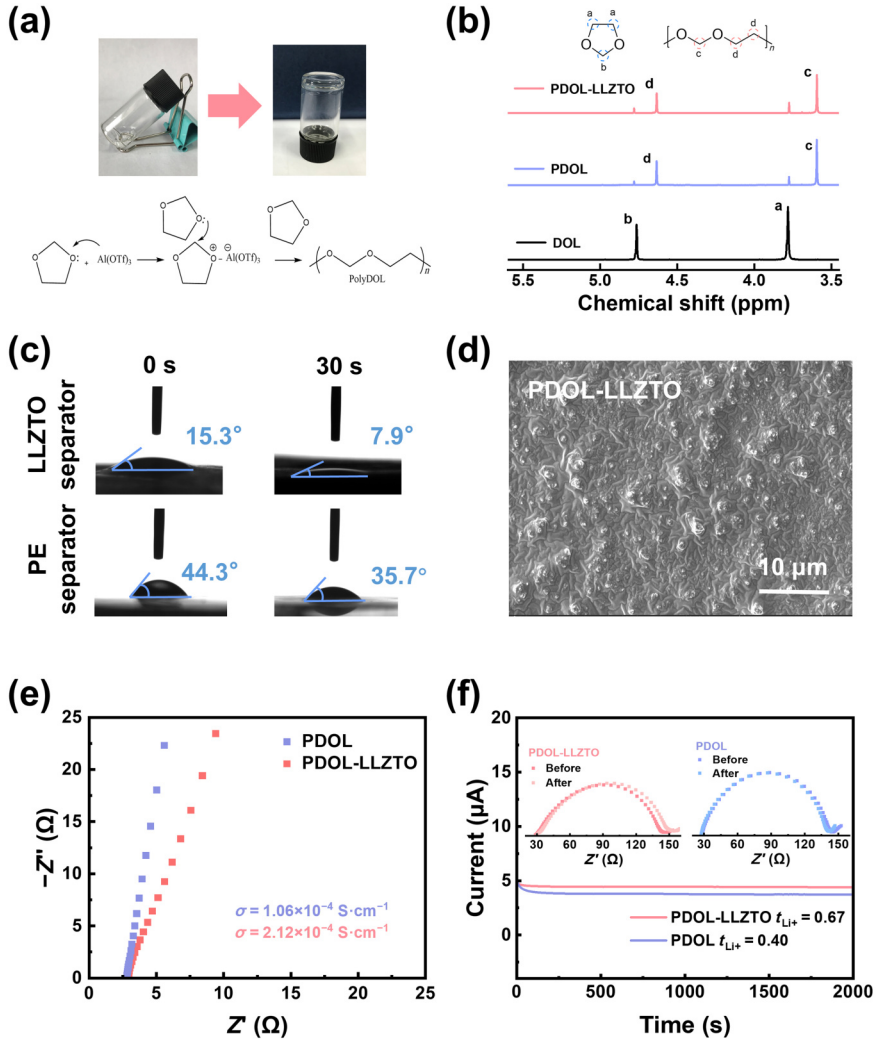

Figure 4 (a) Polymerization mechanism of DOL initiated by $Al(OTf)_3$ and digital images before and after polymerization. (b) ^1H NMR of DOL monomer, PDOL electrolyte, and PDOL-LLZTO hybrid electrolyte. (c) Contact angle test of original PE separator and LLZTO-coated ceramic separator. (d) Surface SEM image of PDOL-LLZTO hybrid electrolyte. (e) Impedance plots of the PDOL and PDOL-LLZTO hybrid electrolytes at room temperature. (f) Chronoamperometry profiles for the PDOL and PDOL-LLZTO hybrid electrolytes at room temperature. The inset figures are impendence plots before and after polarization.

10^{-4} S·cm^{-1}) (Fig. 4(e)). This enhancement is attributed to the improved infiltration of DOL precursors into porous ceramic separators. Moreover, the existence of LLZTO accelerates Li-ion percolation along the LLZTO-PDOL interface. LLZTO fillers, with sufficient surface Lewis base sites, facilitate Li salt dissociation, thereby enhancing the Li carrier concentration (Fig. S7 in the ESM). In addition, LLZTO can capture $TFSI^-$ anions due to the interactions between LLZTO and anions, leading to the immobility of anions. As a result, PDOL-LLZTO hybrid electrolyte exhibit an increased t_{Li^+} of 0.67 (Fig. 4(f)). The enhanced t_{Li^+} indicates reduced concentration polarization, which promotes uniform Li deposition. The linear sweep voltammetry (LSV) measurements further demonstrate an expanded electrochemical window of up to 4.70 V for PDOL hybrid electrolyte compared to 4.00 V for pristine PDOL electrolytes (Fig. S8 in the ESM). These results suggest that ultrathin PDOL hybrid electrolyte hold significant promise for high-energy-density battery applications.

2.3 Interface compatibility and Li deposition behaviours

The compatibility of PDOL hybrid electrolyte with Li metal anode was verified in Li||Li symmetric cells. As shown in Figs. 5(a) and 5(b), the PDOL hybrid electrolyte exhibit a higher critical current density (CCD) of 1.9 mA·cm^{-2} than that of PDOL electrolyte (1.2 mA·cm^{-2}), implying a considerable capability of PDOL hybrid electrolyte in inhibiting Li dendrites. Moreover, the Li|PDOL-LLZTO|Li symmetric cell demonstrates an extended cycling lifespan of 200 h with a steady overpotential of 40 mV at 0.5 mA·cm^{-2} and 0.5 mAh·cm^{-2}. In contrast, a sudden internal short circuit induced by Li dendrite penetration occurs for Li|PDOL|Li symmetric cells after cycling for 100 h (Fig. 5(c)). The electrochemical impedance spectrum measurements were conducted to further evaluate the interface impedance evolution. The Li|PDOL-LLZTO|Li symmetric cells show a reduced initial interface resistance, which remains significantly lower even after cycling (Fig. S9 in the ESM). This result provides strong evidence for good interface compatibility between PDOL-LLZTO hybrid electrolyte and Li metal anode.

The morphologies of the Li metal anode after cycling were also performed (Figs. 5(d) and 5(e), and Fig. S10 in the ESM). Li|PDOL-LLZTO|Li cell shows dense and smooth Li morphologies, while mossy dendrites are observed for the Li|PDOL|Li cell. Moreover, a thinner Li deposition layer is also witnessed in the Li|PDOL-

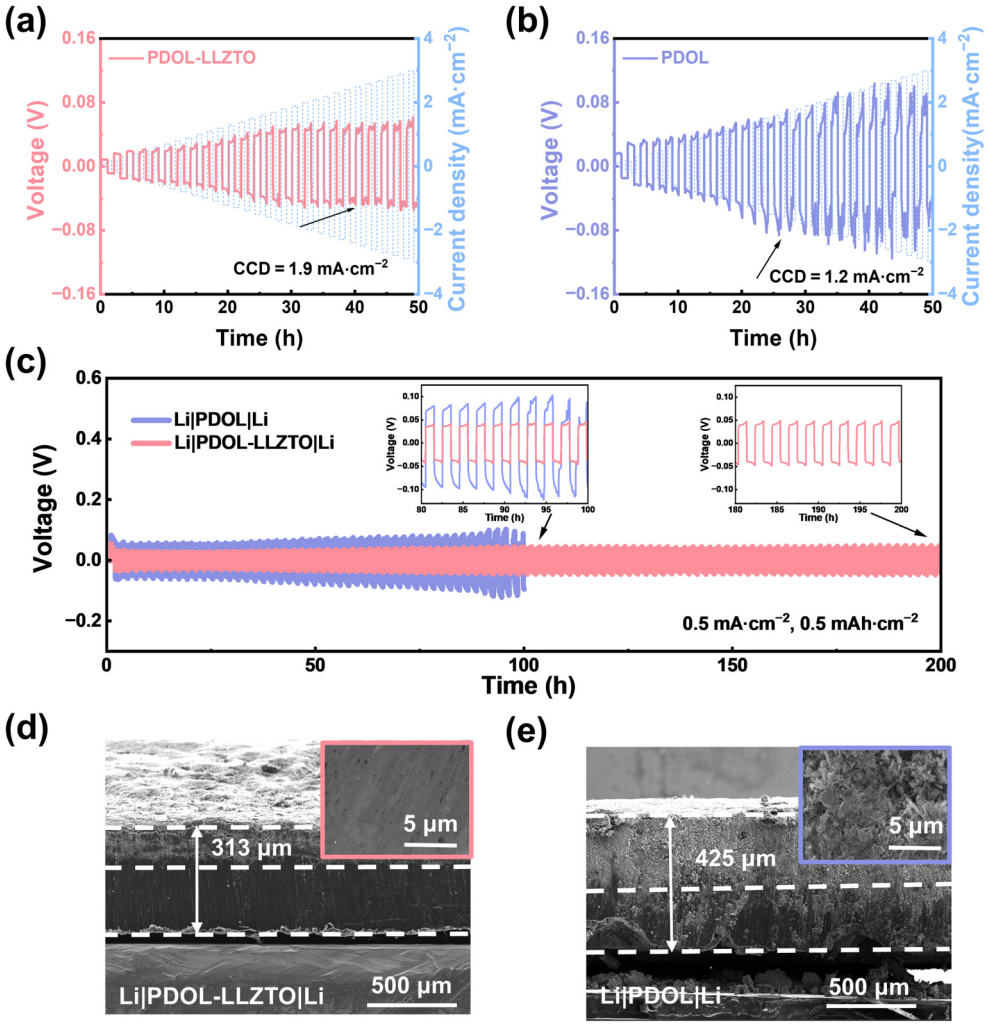

Figure 5 (a) CCD tests of the Li||Li symmetrical cells using (a) the PDOL-LLZTO hybrid electrolyte and (b) the PDOL electrolyte at room temperature. (c) Long-term cycling tests of Li||Li symmetrical cells at 0.5 mA·cm^{-2} and 0.5 mAh·cm^{-2}. The inset images show enlargements of specific parts of the cycles. (d) and (e) SEM images of cross-section and surface morphologies of cycled Li anodes. The insert shows Li surface morphologies.

LLZTO|Li cell, verifying the enhanced interfacial stability and excellent capability in regulating Li deposition and suppressing Li dendrites. Consequently, the presence of the LLZTO layer not only promotes Li transportation but also rectifies the distribution of Li^+. Furthermore, the high-modulus LLZTO layer as a rigid barrier physically suppresses the Li dendrites. Therefore, the PDOL-LLZTO electrolyte induces uniform Li deposition and achieves long-term cycling stability in the Li||Li symmetric cells.

2.4 Electrochemical performances of full cells

To evaluate the performances of PDOL-LLZTO hybrid electrolyte in a practical battery system, Li||LFP full cells were fabricated by *in-situ* polymerization of PDOL. As shown in Fig. 6(a), the Li||LFP cell employing PDOL-LLZTO hybrid electrolyte exhibits enhanced rate capacity at all current densities from 0.1 to 1 C. It is obvious that the discharge capacity of Li|PDOL-LLZTO|LFP cell is higher than the cell employed PDOL, reaching 163.8 mAh·g^{-1} at 0.1 C. When the current density gradually increases to 1 C, the capacity of the Li|PDOL-LLZTO|LFP cell remains 142.0 mAh·g^{-1}, compared to the capacity of the Li|PDOL|LFP cell decaying to only 121.4 mAh·g^{-1}. The capacity of the Li|PDOL-LLZTO|LFP cell quickly recovers to its initial level when the current density returns to 0.1 C (Fig. 6(b)). In contrast, the Li|PDOL|LFP cell shows reduced discharge capacity and rate performance. Long-term cycling tests of Li||LFP cells were also conducted. The Li||LFP cell employing PDOL-LLZTO electrolyte exhibits stable cycling over 320 cycles with an average Coulombic efficiency of 99.59% and a high capacity rention of 93.3% at 0.5 C (Figs. 6(c) and 6(d)). In comparison, the capacity of the Li|PDOL|LFP cell decreases to 130.4 mAh·g^{-1} after 231 cycles. Interestingly, no obvious increase in interface impedance is observed for the Li|PDOL-LLZTO|LFP cell after 320 cycles. Conversely, the Li|PDOL|LFP cell presents an increased trend in the impedance with increasing cycles (Fig. 6(e)). These results indicate the enhanced compatibility of PDOL-LLZTO hybrid electrolyte with Li anode, as well as improved interfacial Li kinetics, which is attributed to fast Li-ion percolation and reduced interface polarization induced by high Li-ion transference number.

To further demonstrate the electrochemical performance of the PDOL-LLZTO hybrid electrolyte under harsh working conditions, the Li||LFP cells cycled at elevated temperatures of 60 °C. The Li|PDOL-LLZTO|LFP cell delivers an initial discharge-specific capacity of up to 159.6 mAh·g^{-1} and retains a discharge capacity of 139.7 mAh·g^{-1} after 100 cycles at 0.5 C, while the Li|PDOL|LFP cell experiences significant capacity decay in the initial cycles (Fig. 6(f)).

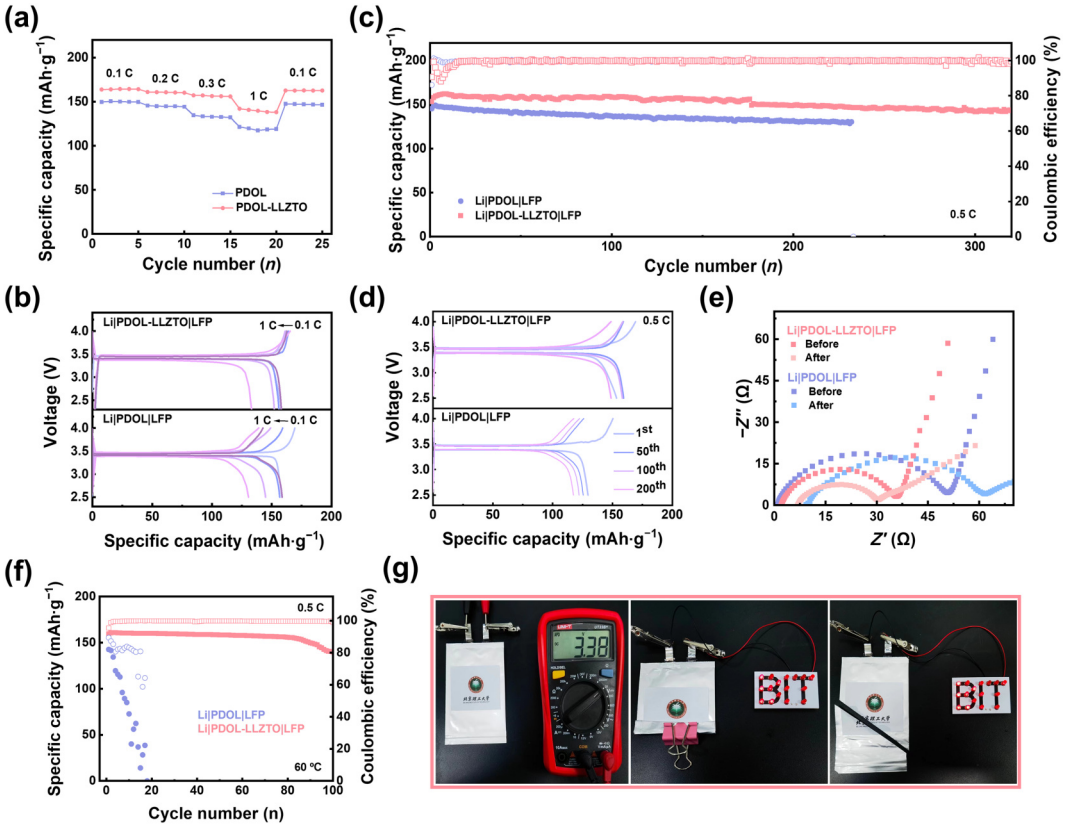

Figure 6 (a) Rate capability and (b) voltage profiles of the Li||LFP cell with PDOL and PDOL-LLZTO electrolytes. (c) Cycling stability and (d) voltage profiles of the Li||LFP cells with PDOL and PDOL-LLZTO electrolytes at 0.5 C at room temperature. (e) Impedance plots of the Li|PDOL|LFP and Li|PDOL-LLZTO|LFP cells before and after cycling. (f) Cycling stability of the Li||LFP cells employing PDOL and PDOL-LLZTO electrolytes at an elevated temperature of 60 °C. (g) Photos of Li|PDOL-LLZTO|LFP pouch cell lighting a red LED under mechanical abuse conditions.

The improved high-temperature performance can be attributed to the enhanced thermal stability of PDOL hybrid electrolyte when coupled with LLZTO due to the strengthened –C–O–C– bond in PDOL induced by the competitive coordination of LLZTO with Li^+. In addition, the prototype Li||LFP pouch cell was also fabricated (Fig. 6(g)). Remarkably, despite being subjected to bending or cutting, the pouch cell was still able to power an light-emitting device (LED) array, demonstrating reliable safety performance and potential for practical application.

Therefore, this work highlights a promising approach to improving the thermal stability of PDOL electrolytes for safe solid-state Li metal batteries through the competitive coordination of Lewis acid–base interactions. In addition to LLZTO, other fillers with Lewis basic sites, such as $Li_{1.5}Al_{0.5}Ge_{1.5}(PO_4)_3$ (LAGP) and $Li_{1.4}Al_{0.4}Ti_{1.6}(PO_4)_4$ (LATP), can also enhance the thermal stability of PDOL-based electrolyte through the competitive coordination mechanism. However, it is essential to thoroughly evaluate their chemical and electrochemical stability with PDOL electrolytes and Li anode. Overall, a bright future of high-safety solid-state Li metal batteries looks promising, but more efforts are still needed.

3 Conclusions

In summary, the competitive coordination mechanism of solvated Li^+ is demonstrated to enhance the thermal stability of PDOL electrolytes. The strong Lewis acid–base interactions between LLZTO and Li^+ weakens the coordination of Li^+ with PDOL chains, resulting in reinforced bond energy of the vulnerable –C–O–C– bonds in PDOL. Consequently, the thermal decomposition temperature of PDOL increases from 110 to 302 °C. An ultrathin PDOL-LLZTO hybrid electrolyte, with a thickness of 12 μm and improved thermal stability, was prepared through *in-situ* polymerization of PDOL within an ultrathin LLZTO-coated separator. Due to the incorporation of LLZTO fillers into PDOL, the ultrathin hybrid electrolyte exhibits enhanced room-temperature ionic conductivity (2.12×10^{-4} S·cm^{-1}) and a high Li^+ transference number (0.67). Li||Li symmetric cells demonstrate an extended cycling life of over 200 h with a low overpotential. Moreover, Li||LFP cells with ultrathin PDOL-LLZTO hybrid electrolyte also cycle stably for over 100 cycles at an elevated working temperature of 60 °C. Therefore, this work provides novel insights to guide the design of thermally stable electrolytes for safe solid-state Li metal batteries.

Electronic Supplementary Material: Supplementary material (further details of the preparation of ultrathin PDOL hybrid electrolyte and materials characterization) is available in the online version of this article at https://doi.org/10.26599/NR.2025.94907220.

Data availability

All data needed to support the conclusions in the paper are presented in the manuscript and the Electronic Supplementary Material. Additional data related to this paper may be requested from the corresponding author upon request.

Acknowledgements

This work is funded by the Beijing Municipal Natural Science Foundation (No. L223009), the National Natural Science Foundation of China (Nos. 22075029, 22209014, and 22479012), the National Key Research and Development Program of China (No. 2021YFB2500300), the Key Research and Development (R&D) Projects of Shanxi Province (No. 2021020660301013), and the Fundamental Research Funds for the Central Universities (No. 2023CX01031).

Declaration of competing interest

All the contributing authors report no conflict of interests in this work.

Author contribution statement

Y.-Y. P.: Data curation, validation, writing manuscripts, experimental design. J.-K. H.: Experimental design, validation. H. Y.: Conceptualization, project administration, funding acquisition, supervision. S.-J. Y., X.-L. W., and Z. L.: Investigation, validation, data curation. J. L.: Supervision, validation. B.-Q. L. and J.-Q. H.: Funding acquisition, supervision. All the authors have approved the final manuscript.

Use of AI statement

None.

References

[1] Sun, C. W.; Liu, J.; Gong, Y. D.; Wilkinson, D. P.; Zhang, J. J. Recent advances in all-solid-state rechargeable lithium batteries. *Nano Energy* **2017**, *33*, 363–386.

[2] Liao, Y. L.; Hu, J. K.; Fu, Z. H.; Zhao, C. Z.; Lu, Y.; Li, S.; Yang, S. J.; Sun, S.; Wang, X. L.; Liu, J. et al. Integrated interface configuration by *in-situ* interface chemistry enabling uniform lithium deposition in all-solid-state lithium metal batteries. *J. Energy Chem.* **2023**, *80*, 458–465.

[3] Liu, J.; Yuan, H.; Liu, H.; Zhao, C. Z.; Lu, Y.; Cheng, X. B.; Huang, J. Q.; Zhang, Q. Unlocking the failure mechanism of solid state lithium metal batteries. *Adv. Energy Mater.* **2022**, *12*, 2100748.

[4] Li, M.; Lu, J.; Chen, Z. W.; Amine, K. 30 years of lithium-ion batteries. *Adv. Mater.* **2018**, *30*, 1800561.

[5] Harper, G.; Sommerville, R.; Kendrick, E.; Driscoll, L.; Slater, P.; Stolkin, R.; Walton, A.; Christensen, P.; Heidrich, O.; Lambert, S. et al. Recycling lithium-ion batteries from electric vehicles. *Nature* **2019**, *575*, 75–86.

[6] Liu, J.; Mei, X. W.; Peng, F. Lignin derived porous carbon with favorable mesoporous contributions for highly efficient ionic liquid-based supercapacitors. *Chin. Chem. Lett.* **2023**, *34*, 108187.

[7] Wu, Y. J.; Wang, S.; Li, H.; Chen, L. Q.; Wu, F. Progress in thermal stability of all-solid-state-Li-ion-batteries. *InfoMat* **2021**, *3*, 827–853.

[8] Feng, X. N.; Ouyang, M. G.; Liu, X.; Lu, L. G.; Xia, Y.; He, X. M. Thermal runaway mechanism of lithium ion battery for electric vehicles: A review. *Energy Storage Mater.* **2018**, *10*, 246–267.

[9] Yang, S. J.; Hu, J. K.; Jiang, F. N.; Cheng, X. B.; Sun, S.; Hsu, H. J.; Ren, D. S.; Zhao, C. Z.; Yuan, H.; Ouyang, M. G. et al. Oxygen-induced thermal runaway mechanisms of Ah-level solid-state lithium metal pouch cells. *eTransportation* **2023**, *18*, 100279.

[10] He, L. J.; Liu, J.; Lv, T. T.; Wei, A. C.; Yuan, T. Q. 1T-rich MoS_2 nanosheets anchored on conductive porous carbon as effective polysulfide promoters for lithium-sulfur batteries. *J. Colloid Interface Sci.* **2024**, *671*, 175–183.

[11] Chang, C.; Chen, W.; Chen, Y.; Chen, Y. H.; Chen, Y.; Ding, F.; Fan, C. H.; Fan, H. J.; Fan, Z. X.; Gong, C. et al. Recent progress on two-dimensional materials. *Acta Phys. Chim. Sin.* **2021**, *37*, 2108017.

[12] Wu, J. Y.; Zeng, H. X.; Shi, Q. X.; Li, X. W.; Xia, Q.; Xue, Z. G.; Ye, Y. S.; Xie, X. L. Safety-reinforced plastic crystal composite polymer electrolyte by 3D MoS_2-based nano-hybrid for Li-metal batteries. *J. Power Sources* **2018**, *405*, 7–17.

[13] Li, S.; Yang, S. J.; Liu, G. X.; Hu, J. K.; Liao, Y. L.; Wang, X. L.; Wen, R.; Yuan, H.; Huang, J. Q.; Zhang, Q. A dynamically stable mixed conducting interphase for all-solid-state lithium metal batteries. *Adv. Mater.* **2024**, *36*, 2307768.

[14] Hu, J. K.; Yuan, H.; Yang, S. J.; Lu, Y.; Sun, S.; Liu, J.; Liao, Y. L.; Li, S.; Zhao, C. Z.; Huang, J. Q. Dry electrode technology for scalable and flexible high-energy sulfur cathodes in all-solid-state lithium-sulfur batteries. *J. Energy Chem.* **2022**, *71*, 612–618.

[15] Li, S.; Zhang, S. Q.; Shen, L.; Liu, Q.; Ma, J. B.; Lv, W.; He, Y. B.; Yang, Q. H. Progress and perspective of ceramic/polymer composite solid electrolytes for lithium batteries. *Adv. Sci.* **2020**, *7*, 1903088.

[16] Deng, B.; Jing, M. X.; Li, R.; Li, L. X.; Yang, H.; Liu, M. Q.; Xiang, J.; Yuan, W. Y.; Shen, X. Q. Integrating high ionic conductive PDOL solid/gel composite electrolyte for enhancement of interface combination and lithium dentrite inhibition of solid-state lithium battery. *J. Colloid Interface Sci.* **2022**, *620*, 199–208.

[17] Yao, P. H.; Yu, H. B.; Ding, Z. Y.; Liu, Y. C.; Lu, J.; Lavorgna, M.; Wu, J. W.; Liu, X. J. Review on polymer-based composite electrolytes for lithium batteries. *Front. Chem.* **2019**, *7*, 522.

[18] S. H.; Xie, B.; Zhuang, X. C.; Wang, S. T.; Qiao, L. X.; Dong, S. M.; Ma, J.; Zhou, Q.; Zhang, H. R.; Zhang, J. J. et al. Great challenges and new paradigm of the *in situ* polymerization technology inside lithium batteries. *Adv. Funct. Mater.* **2024**, *34*, 2314063.

[19] Xu, P.; Shuang, Z. Y.; Zhao, C. Z.; Li, X.; Fan, L. Z.; Chen, A. B.; Chen, H. T.; Kuzmina, E.; Karaseva, E.; Kolosnitsyn, V. et al. A review of solid-state lithium metal batteries through *in-situ* solidification. *Sci. China Chem.* **2024**, *67*, 67–86.

[20] Yang, H.; Jing, M. X.; Wang, L.; Xu, H.; Yan, X. H.; He, X. M. PDOL-based solid electrolyte toward practical application: Opportunities and challenges. *Nano-Micro Lett.* **2024**, *16*, 127.

[21] Wang, Z. L.; Wang, Y. H.; Shen, L. Y.; Jin, Z. Q.; Law, H. M.; Wang, A. B.; Wang, W. K.; Ciucci, F. Towards durable practical lithium-metal batteries: Advancing the feasibility of poly-DOL-based quasi-solid-state electrolytes via a novel nitrate-based additive. *Energy Environ. Sci.* **2023**, *16*, 4084–4092.

[22] Liu, Q.; Cai, B. Y.; Li, S.; Yu, Q. P.; Lv, F. Z.; Kang, F. Y.; Wang, Q.; Li, B. H. Long-cycling and safe lithium metal batteries enabled by the synergetic strategy of *ex situ* anodic pretreatment and an in-built gel polymer electrolyte. *J. Mater. Chem. A* **2020**, *8*, 7197–7204.

[23] Liu, Y. L.; Xu, Y. L. Porous membrane host-derived *in-situ* polymer electrolytes with double-stabilized electrode interface enable long cycling lithium metal batteries. *Chem. Eng. J.* **2022**, *433*, 134471.

[24] Li, L. X.; Li, R.; Huang, Z. H.; Yang, H.; Liu, M. Q.; Xiang, J.; Hussain, S.; Shen, X. Q.; Jing, M. X. A multifunctional gradient solid electrolyte remarkably improving interface compatibility and ion transport in solid-state lithium battery. *ACS Appl. Mater. Interfaces* **2022**, *14*, 30786–30795.

[25] Yang, H.; Zhang, B.; Jing, M. X.; Shen, X. Q.; Wang, L.; Xu, H.; Yan, X. H.; He, X. M. *In situ* catalytic polymerization of a highly homogeneous PDOL composite electrolyte for long-cycle high-voltage solid-state lithium batteries. *Adv. Energy Mater.* **2022**, *12*, 2201762.

[26] Li, W.; Gao, J.; Tian, H. Y.; Li, X. L.; He, S.; Li, J. P.; Wang, W. L.; Li, L.; Li, H.; Qiu, J. S. et al. SnF_2-catalyzed formation of polymerized dioxolane as solid electrolyte and its thermal decomposition behavior. *Angew. Chem., Int. Ed.* **2022**, *61*, e202114805.

[27] Cui, J.; Du, Y. F.; Zhao, L.; Li, X. C.; Sun, Z. X.; Li, D.; Li, H.

Thermal stable poly-dioxolane based electrolytes via a robust crosslinked network for dendrite-free solid-state Li-metal batteries. *Chem. Eng. J.* **2023**, *461*, 141973.

[28] Luo, M. Z.; Su, Y.; Sun, Z. F.; Yu, X. Y.; He, Z. N.; Zhou, J.; Yan, R. T.; Wang, M. S.; Li, Y. X.; Yang, Y. Unveiling the thermal decomposition mechanism of high-nickel cathode with loaded nano-Al_2O_3 on conductive carbon for safe lithium-ion batteries. *Energy Storage Mater.* **2024**, *67*, 103256.

[29] Roganović, A.; Vraneš, M.; Cvjetićanin, N.; Chen, X. P.; Papović, S. Effect of zwitterionic additive on electrode protection through electrochemical performances of anatase TiO_2 nanotube array electrode in ionic liquid electrolyte. *Int. J. Mol. Sci.* **2023**, *24*, 3495.

[30] Ma, Q.; Yue, J. P.; Fan, M.; Tan, S. J.; Zhang, J.; Wang, W. P.; Liu, Y.; Tian, Y. F.; Xu, Q.; Yin, Y. X. et al. Formulating the electrolyte towards high-energy and safe rechargeable lithium-metal batteries. *Angew. Chem., Int. Ed.* **2021**, *60*, 16554–16560.

[31] Zhang, X.; Liu, T.; Zhang, S. F.; Huang, X.; Xu, B. Q.; Lin, Y. H.; Xu, B.; Li, L. L.; Nan, C. W.; Shen, Y. Synergistic coupling between $Li_{6.75}La_3Zr_{1.75}Ta_{0.25}O_{12}$ and poly(vinylidene fluoride) induces high ionic conductivity, mechanical strength, and thermal stability of solid composite electrolytes. *J. Am. Chem. Soc.* **2017**, *139*, 13779–13785.

[32] Kim, J. S.; Yoon, G.; Kim, S.; Sugata, S.; Yashiro, N.; Suzuki, S.; Lee, M. J.; Kim, R.; Badding, M.; Song, Z. et al. Surface engineering of inorganic solid-state electrolytes via interlayers strategy for developing long-cycling quasi-all-solid-state lithium batteries. *Nat. Commun.* **2023**, *14*, 782.

[33] Jia, M. Y.; Zhao, N.; Huo, H. Y.; Guo, X. X. Comprehensive investigation into garnet electrolytes toward application-oriented solid lithium batteries. *Electrochem. Energy Rev.* **2020**, *3*, 656–689.

[34] Shen, F.; Guo, W. C.; Zeng, D. Y.; Sun, Z. T.; Gao, J.; Li, J.; Zhao, B.; He, B.; Han, X. G. A simple and highly efficient method toward high-density garnet-type LLZTO solid-state electrolyte. *ACS Appl. Mater. Interfaces* **2020**, *12*, 30313–30319.

[35] Hu, J. K.; Gao, Y. C.; Yang, S. J.; Wang, X. L.; Chen, X.; Liao, Y. L.; Li, S.; Liu, J.; Yuan, H.; Huang, J. Q. High energy density solid-state lithium metal batteries enabled by *in situ* polymerized integrated ultrathin solid electrolyte/cathode. *Adv. Funct. Mater.* **2024**, *34*, 2311633.

[36] Chen, M. H.; Yue, Z. Y.; Wu, Y. X.; Wang, Y.; Li, Y.; Chen, Z. Thermal stable polymer-based solid electrolytes: Design strategies and corresponding stable mechanisms for solid-state Li metal batteries. *Sustain. Mater. Technol.* **2023**, *36*, e00587.

[37] Zhao, Q.; Liu, X. T.; Stalin, S.; Khan, K.; Archer, L. A. Solid-state polymer electrolytes with in-built fast interfacial transport for secondary lithium batteries. *Nat. Energy* **2019**, *4*, 365–373.